

Article

Effect of Sigma Phases on Moderate-Temperature Tensile Properties of Z3CN20.09M CASS Used for Primary Coolant Pipe of Nuclear Power Plant

Yongqiang Wang ¹, Chaojun Hu ¹, Na Li ^{2,*}, Suhua Lin ¹, Zhangqi Ge ¹ and Chengsi Zheng ¹¹ School of Materials Science and Engineering, Anhui University of Technology, Maanshan 243002, China² School of Metallurgical Engineering, Anhui University of Technology, Maanshan 243002, China

* Correspondence: linaustb@163.com; Tel.: +86-0555-2311571

Abstract: The effect of sigma phases on the moderate-temperature tensile properties of Z3CN20.09M casting austenite stainless steel was investigated by means of isothermal treatment, scanning electron microscopy, transmission electron microscopy, instrumented nanoindentation, tensile testing, and finite element simulation. The results show that the yield strength and ultimate tensile strength of aged specimens tensile tested at moderate temperature increase remarkably with an increasing sigma phase, while the elongation at break decreased. The strain-hardening rate of aged specimens with sigma phases is higher than that of unaged specimens without sigma phases at a certain low-strain range. However, the value of the strain-hardening rate of aged specimens is lower than that of unaged specimens when the strain exceeds a certain value. The effect of the sigma phase on the tensile properties at moderate temperature is also more significant. This can be attributed to the many high-energy σ/γ_2 and $\alpha/\sigma/\gamma_2$ incoherent phase boundaries caused by the precipitation of sigma phases. On the one hand, these boundaries hinder the movement of dislocations and subsequently accumulate dislocations to some extent, so strength is enhanced and the strain-hardening rate is improved. On the other hand, microcracks at these interfaces initiate and propagate more easily when the strain exceeds a certain value. Thus, the elongation value and the strain-hardening rate decrease.

Keywords: sigma phase; casting austenite stainless steel; tensile testing at moderate temperature; strength and plasticity; strain-hardening rate



Citation: Wang, Y.; Hu, C.; Li, N.; Lin, S.; Ge, Z.; Zheng, C. Effect of Sigma Phases on Moderate-Temperature Tensile Properties of Z3CN20.09M CASS Used for Primary Coolant Pipe of Nuclear Power Plant. *Coatings* **2023**, *13*, 101. <https://doi.org/10.3390/coatings13010101>

Academic Editor: Paolo Castaldo

Received: 6 December 2022

Revised: 1 January 2023

Accepted: 3 January 2023

Published: 5 January 2023



Copyright: © 2023 by the authors. Licensee MDPI, Basel, Switzerland. This article is an open access article distributed under the terms and conditions of the Creative Commons Attribution (CC BY) license (<https://creativecommons.org/licenses/by/4.0/>).

1. Introduction

Nuclear power is one of the most important and popular types of energy used to reduce carbon dioxide emissions due to its characteristics of being clean and efficient, having low cost, and being only affected by the area or weather to a limited extent. The primary coolant pipe, as one of the key structural components in the nuclear island of a nuclear power plant, seals the high temperature and pressure, radioactive, and corrosive coolant; maintains and restricts the coolant circulation flow; and plays an important role in ensuring the safety and normal operation of the reactor. It is always manufactured from cast austenitic stainless steel (CASS), for instance Z3CN20.09M, characterized by an austenite–ferrite dual-phase microstructure, which has outstanding mechanical, high resistance to stress corrosion cracking, and processing properties [1–5].

The ferrite phases in CASS improve strength, reduce hot cracking during welding, and enhance the resistance to stress corrosion cracking. However, they also lead to thermal aging embrittlement or sensitization when the primary coolant pipes are heat-treated or welded in the manufacturing process [6–10]. The precipitation of M₂₃C₆ carbide-, chi-, and sigma-phase intermetallic compounds in stainless steel is the main reason for this sensitization [11–13]. These precipitated phases negatively impact both the mechanical properties and the corrosion resistance. It is well known that the sigma phase is the most harmful among all the precipitates mentioned above. Many studies focused on sigma

phases have been conducted in recent decades. The effect of sigma phases on mechanical properties, including strength, toughness, creep, wear resistance, etc. [14–22], is one of most important aspects among these studies. Chen et al. [14] found that the impact toughness of SAF2205 duplex stainless steel was sensitive to the precipitation of sigma phase, even at the initial stage of aging, and that the impact energy of aged specimens at 650–975 °C decreased significantly with increasing aging times. Liu [15] studied the effect of sigma-phase precipitation on the mechanical properties of S32205 duplex stainless steel and found that the formed sigma phase in S32205 duplex stainless steel led to an obvious increase in the hardness, a certain increase in the strength, and a sharp decrease in the ductility. Pohl et al. [16] also proved that sigma-phase precipitation can improve the tensile strength of stainless steel. Shek et al. [17] showed that the yield strengths and ultimate tensile strengths of 25Cr-8Ni duplex stainless steel tensile tested at 550 and 750 °C increased, while the ductility decreased in all aged samples compared with the unaged ones.

Although more research has been conducted on the effect of sigma phases on the mechanical properties of stainless steel, previous work mainly focused on the room-temperature or high-temperature mechanical properties of duplex stainless steel or austenite stainless steel. There are very few reports on the effect of sigma phases on the moderate-temperature mechanical properties of CASS with fewer ferrite phases. On the one hand, the mechanism and law of effect of sigma phases on moderate-temperature mechanical properties still needs to be investigated and revealed. On the other hand, a primary coolant pipe is usually serviced at a temperature of approximately 300 °C, possibly nearing 350 °C on the hot end. A study on the effect of sigma phases on the moderate-temperature mechanical properties of CASS is beneficial to compressively evaluating the safety of primary coolant pipes during use. Z3CN20.09M CASS, in which 12–18 vol% is ferrite phase, is widely used for a primary coolant pipe of the pressurized water reactor of nuclear power plants. There have been almost no reports about the effect of sigma phases on moderate-temperature mechanical properties of Z3CN20.09M CASS, although many previous studies have been investigated the corrosion and thermal aging embrittlement behavior, or other mechanical properties, for instance, wearing and low cycle fatigue properties [4,9,20,23–26]. Thus, this work studies the effect of sigma phases on the tensile properties of a Z3CN20.09M CASS in the hope of revealing the mechanism behind the effect of sigma phases, providing some guidance on the development of more outstanding stainless steel used for primary coolant pipes, and a comprehensive evaluation of the safe service of nuclear power plants.

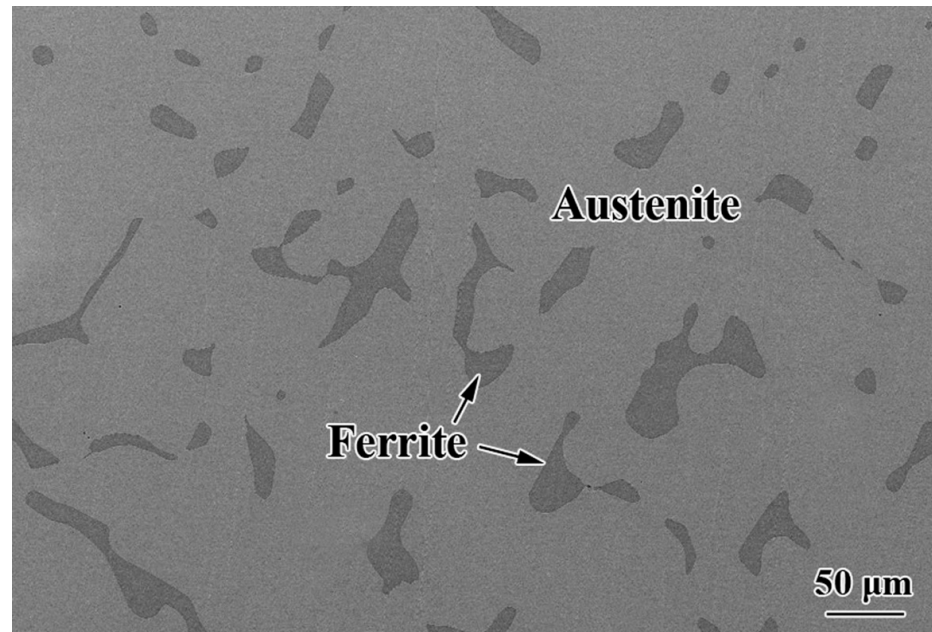
2. Materials and Methods

The studied stainless steel was cut from a piece of a primary coolant pipe. Its chemical composition is listed in Table 1. The pipe was fabricated first by electric-arc and argon-oxygen decarburization melting and then by sand casting and solution treatment (1180 °C, 8 h), followed by water quenching. The microstructure of the as-received Z3CN20.09M CASS is shown in Figure 1. As-received specimens were first isothermally aged at 750 °C for 0–200 h in a resistance furnace, followed by water quenching, and were then cut into different shapes and sizes for the microstructural examination and tensile tests.

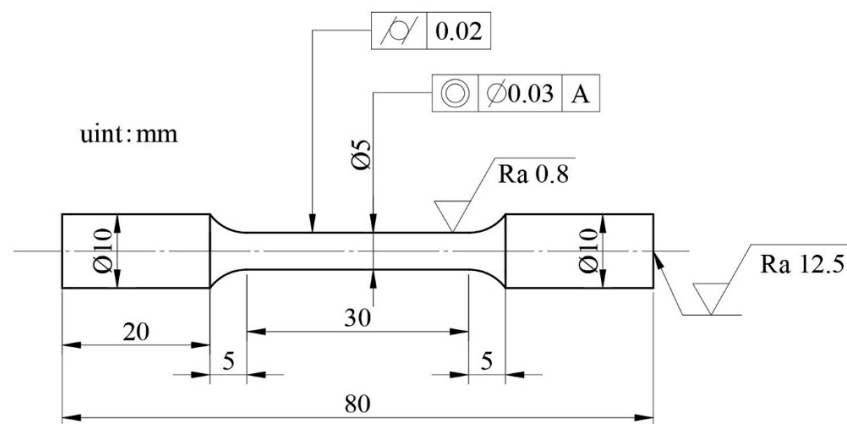
The 10 mm × 10 mm × 10 mm aged specimens were abraded using silicon carbide abrasive paper up to 2000# and then polished with a 1.5 µm diamond paste. The polished specimens were then electrochemically etched for 10 s in a 20 mass% NaOH distilled water solution under 3V direct voltage to differentiate the ferrite, austenite, and sigma phases. The microstructures of all specimens after etching in the electrolyte were observed by scanning electron microscopy (SEM, SUPRA55, ZEISS, Oberkochen, Germany). The sigma phase was further detected with transmission scanning microscopy (TEM, JEM-2010, JEOL, Tokyo, Japan). From the aged specimens, 10 mm × 10 mm × 0.5 mm square specimens were cut, then ground to 40–50 µm thickness, and subsequently prepared as Φ3 mm disc specimens with a small hole puncher. Finally, the TEM specimens were prepared from these Φ3 mm disc specimens using Two Jet Thinning in a 5% perchloric acid alcohol solution.

Table 1. Chemical composition of the Z3CN20.09M cast austenite stainless steel (wt%).

C	Si	Mn	P	S	Cr	Ni	Cu	Co	Nb + Ta	Mo	N	Ti	Fe
0.024	1.09	1.11	0.023	0.0039	20.16	9.06	0.031	0.026	0.066	0.26	0.033	0.0027	balance

**Figure 1.** SEM microstructure of as-received Z3CN20.09M cast austenite stainless steel.

The volume fractions of the sigma phases were estimated based on a counting analysis of the 20 scanning electron microscopy micrographs of the specimens for each condition in a quantitative metallography analysis software (Image-Pro Plus6.0, Media Cybernetics, Rockville, MD, USA). Cylindrical specimens with a diameter of 5 mm and a gage length of 25 and 30 mm, as shown in Figures 2 and 3, were machined for room- and moderate-temperature tensile tests, respectively. The room-temperature tensile tests were performed by a CMT4105 tensile testing machine (MTS-SANS, Shenzhen, China) with a strain rate of $1 \times 10^{-3} \text{ s}^{-1}$. Moderate-temperature tensile tests were conducted at 350 °C on a DDL50 testing machine (Sinotest, Changchun, China) at an initial strain rate of $1 \times 10^{-3} \text{ s}^{-1}$.

**Figure 2.** Geometry and size of specimens used for room-temperature tensile tests.

The elastic moduli of the ferrite, austenite, and sigma phases in aged Z3CN20.09M CASS specimens were tested using an Agilent G200 Nanoindentation instrument (KLA, Oak Ridge, TN, USA) with a maximum load of 700 mN, an indentation at a depth of

40 μm , and a load accuracy of 75 nN. The stress distribution of specimens with and without sigma phases was calculated and simulated in ABAQUS finite element method (FEM) software (6.10, HKS, Providence, RI, USA) with a tensile rate of $1 \times 10^{-3} \text{ s}^{-1}$ after 300 s. ABAQUS software is a convenient simulation software for users to numerically simulate most engineering problems by providing only the geometric shapes, material properties, boundary conditions and load, etc. For nonlinear problems, ABAQUS can select and adjust the convergence criteria and load increase automatically; thus, the accuracy of the calculation can be ensured. The geometry, mesh model, and FEM analysis modeling process are shown in Figure 4. Poisson’s ratio of Z3CN20.09M CASS is 0.28. The elastic moduli of the ferrite, austenite, and sigma phases are 220, 200, and 300 GPa, respectively, according to the nanoindentation test results, as shown in Figure 5. During the calculation, the corners of the left and right boundaries of the mesh model are fixed and, then, a load with a rate of 0.001 mm/s is applied at the left and right boundaries, with the boundary conditions $UR3 = 0, V1 = 0.001/\text{s}$, and $V2 = 0$.

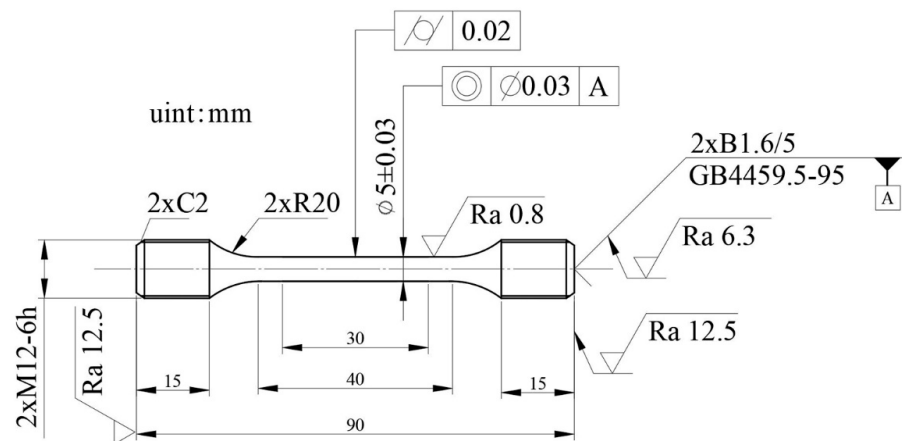


Figure 3. Geometry and size of specimens used for moderate-temperature tensile tests at 350 °C.

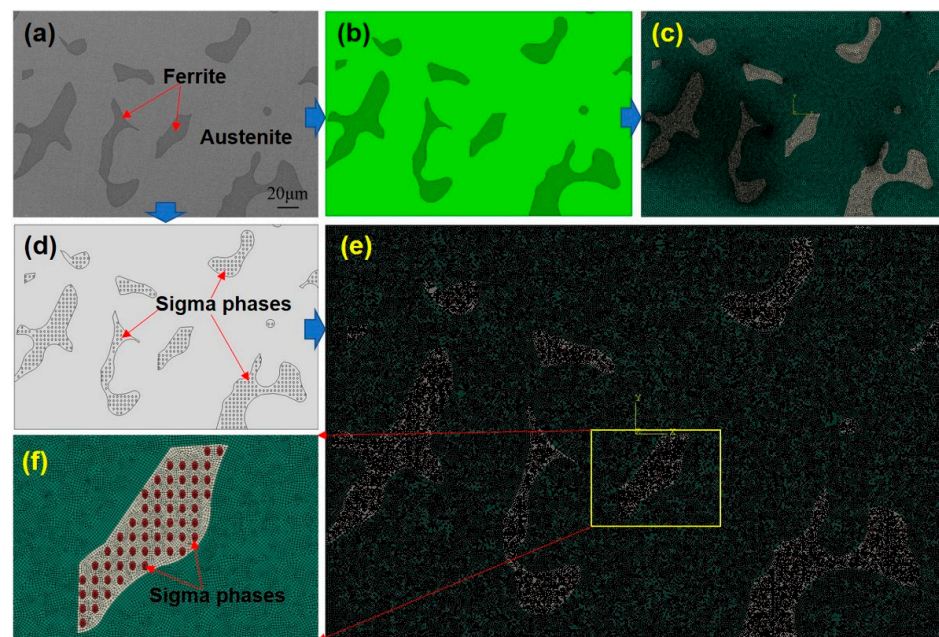


Figure 4. Geometrical and meshed models for ABAQUS finite element software calculating unaged specimens (a–c) without sigma phases and aged specimens with sigma phases. (d) model diagram of calculation; (e) grid division diagram; (f) higher magnification image of localized frame in (e).

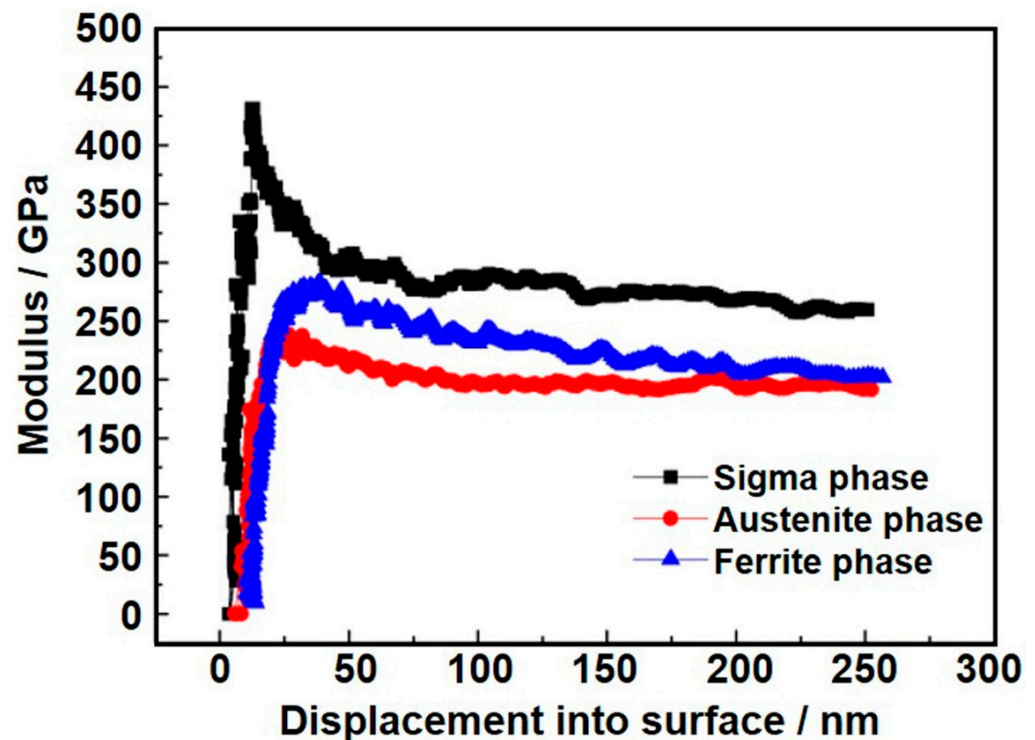


Figure 5. Moduli of sigma, austenite, and ferrite phases in aged Z3CN20.09M specimens at 750 °C for 200 h examined by nanoindentation.

3. Results

3.1. Microstructures of Aged Z3CN20.09M Specimens

Figure 6 shows the microstructures of Z3CN20.09M specimens aged at 750 °C for 0–200 h. Many sigma phases precipitated in the aged specimens when aging time exceeded 50 h. The morphology and structure of the sigma can be seen in the TEM images and diffraction pattern, as shown in Figure 7, showing a tetragonal structure. The content of the sigma phases in aged Z3CN20.09M specimens increased with increasing aging time. However, no significant increase in sigma phase content was seen when aging time exceeded 50 h, as shown in Figure 8. This means that the precipitation of the sigma phase in specimens aged at 750 °C for 50 h has almost been completed and only a coarsening of the phase takes place for long durations of aging, from 50 to 200 h. The higher magnification SEM images displayed larger sigma particles with increased aging time, as shown in Figure 9. The formation of a sigma phase occurs through the eutectoid decomposition of ferrite $\alpha \rightarrow \sigma + \gamma_2$, which is affected by the composition of the steel and the concentration of Cr in the ferrite and austenite phases. A previous study showed maximum kinetics during the precipitation of the sigma phases in the Z3CN20.09M specimens aged at 750 °C, with the fastest precipitation velocity for sigma phases occurring at 750 °C [22]. Therefore, the precipitation of sigma is possible in Z3CN20.09M specimens aged at 750 °C for 50 h.

3.2. Moderate-Temperature Tensile Properties of Aged Z3CN20.09M Specimens

The 350 °C tensile test results of aged Z3CN20.09M specimens at 750 °C for 50, 100, and 200 h are shown in Figure 10a,b. The yield strength (YS) and ultimate tensile strength (UTS) increased with increasing aging times, from 126.9 and 330.7 MPa for unaged specimens to 177.9 and 385.8 MPa for aged specimens after 200 h, respectively, while the elongation percentage at break decreased gradually from 42.3% for unaged specimens to 25.8% for aged specimens after 200 h, as shown in Figure 9a,b. In addition, the elastic modulus of aged specimens is higher than that of unaged specimens. Moreover, the YS, UTS, and elongation of Z3CN20.09M specimens tensile tested at 350 °C are lower than those of specimens at room temperature, as shown in Figure 10c. It is worth noting that the degree

of increase in strength with aging times at 350 °C is higher than that at room temperature (see Table 2). The increases in UTS and YS at room temperature for aged and unaged Z3CN20.09M specimens are 4.0% and 17.5%, respectively. However, the increases in UTS and YS at 350 °C are 16.4% and 40.2%, respectively. It can be seen that the effect of sigma phases on the tensile strength of Z3CN20.09M CASS at 350 °C is more significant than that at room temperature. This means that the strength at moderate-temperature Z3CN20.09M CASS is more sensitive to sigma phases.

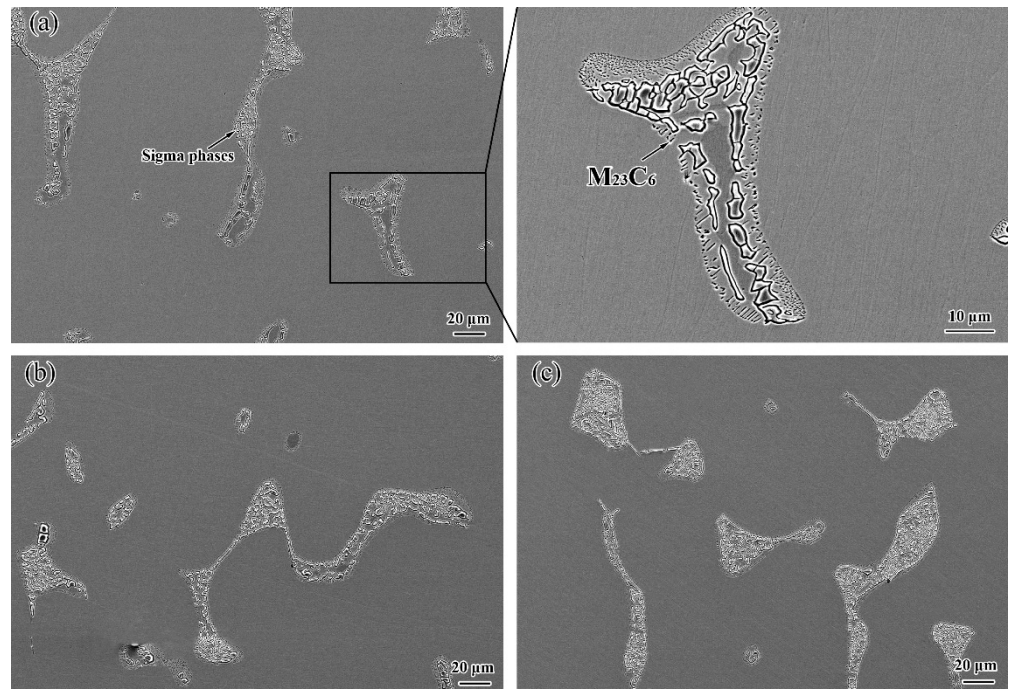


Figure 6. SEM microstructures of Z3CN20.09M specimens aged at 750 °C for different durations: (a) 50 h, (b) 100 h, (c) 200 h.

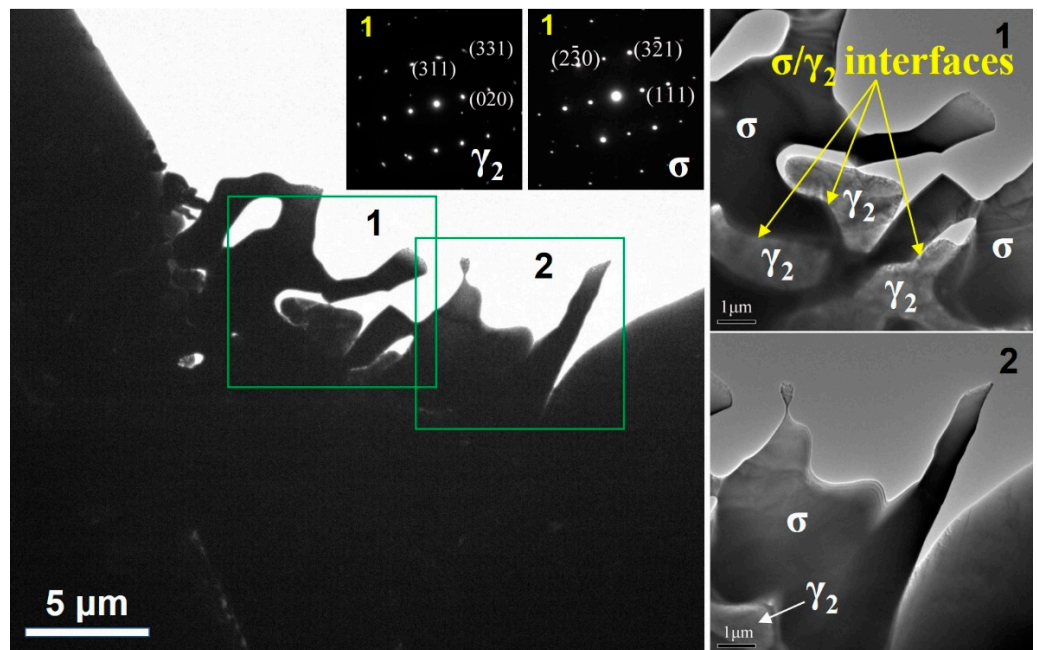


Figure 7. TEM images of the sigma phase in Z3CN20.09M specimens aged at 750 °C for 200 h, with the corresponding selected area electron diffraction patterns in the insets.

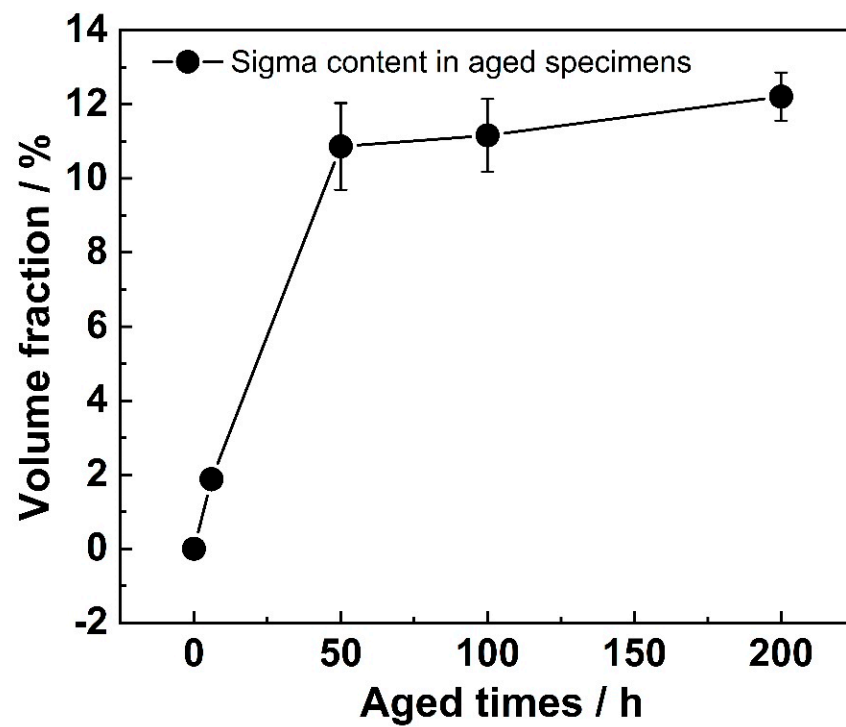


Figure 8. Variation in sigma content in Z3CN20.09M CASS specimens aged at 750 °C with aging times.

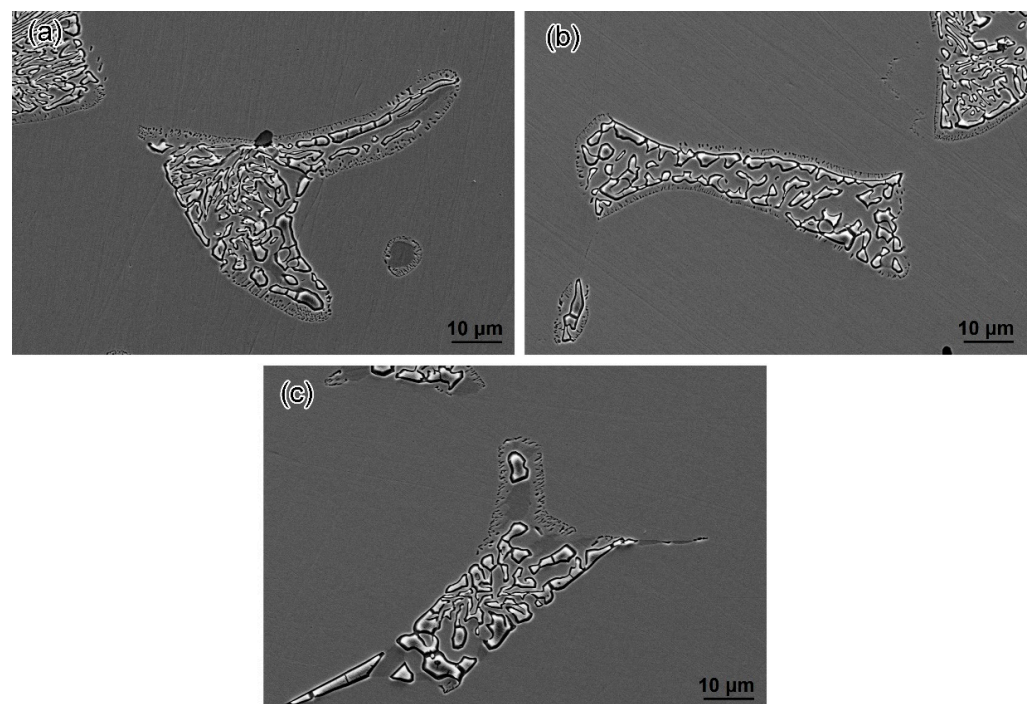


Figure 9. Higher magnification SEM microstructures of Z3CN20.09M specimens aged at 750 °C for different durations: (a) 50 h, (b) 100 h, (c) 200 h.

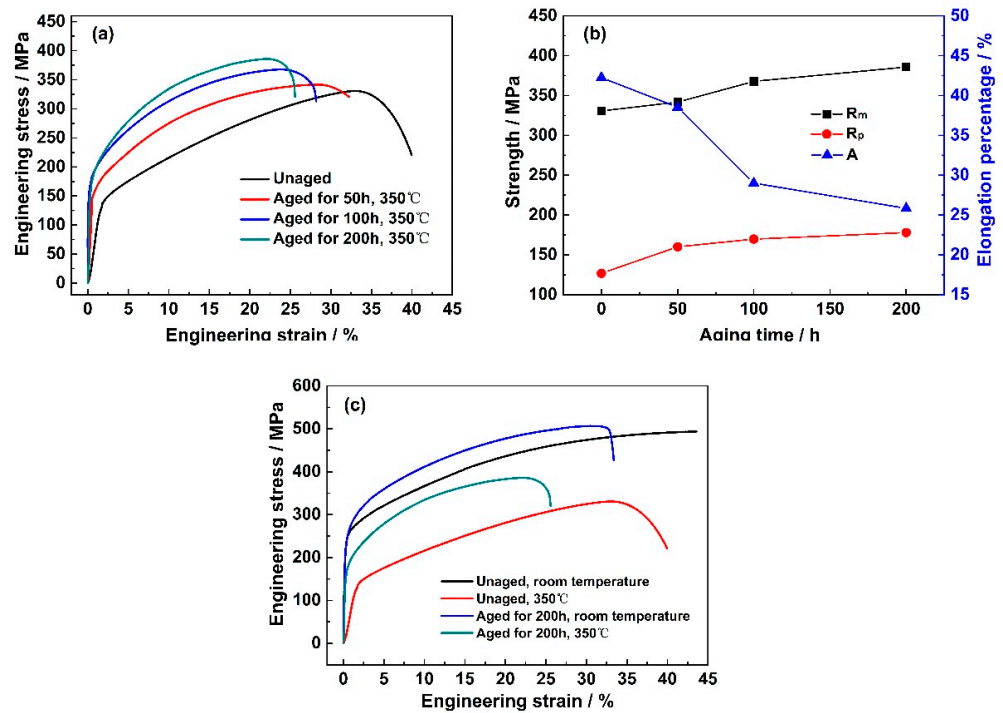


Figure 10. Engineering stress–strain curves of Z3CN20.09M specimens tested at 350 °C (a), the relationship between strength, elongation, and aging times (b), and engineering stress–strain curves of unaged and aged Z3CN20.09M specimens at room temperature and 350 °C (c).

Table 2. Tensile properties of unaged and aged Z3CN20.09M specimens at room and moderate temperature for 200 h.

Temperature	Specimens	Ultimate Tensile Strength/MPa	Percent Increase/%	Yield Strength/MPa	Percent Increase/%	Elongation/%	Percent Decrease/%
RT	Unaged	495.1		234.3		50.3	
	Aged	514.8	4.0	275.2	17.5	40.4	19.7
350 °C	Unaged	330.7		126.9		42.3	
	Aged	385.8	16.4	177.9	40.2	25.8	39.0

3.3. Fracture Morphology of Unaged and Aged Z3CN20.09M Specimens after Moderate-Temperature Tensile Test

The fracture morphologies of unaged and aged Z3CN20.09M specimens after tensile tests at 350 °C are shown in Figure 11. Serious necking appeared in the fracture surfaces of unaged specimens; however, almost no necking appeared in the fracture surface of aged specimens at 750 °C for 200 h, as shown in Figure 11a-1 and b-1. From the fracture morphologies (shown at high magnifications in Figure 11a-2, a-3, b-2 and b-3), many ductile dimples are also seen in the fracture of unaged specimens, which exhibited typical ductile fracture characteristics, while many brittle dissociation fracture surfaces are seen in the fracture of aged specimens, which show characteristics of a brittle fracture as a whole. Even if some ductile fracture zones can be observed, a brittle zone is also seen in the sigma phase, as shown in Figure 11b-3. The EDS measurements of the similar region shown in Figure 11b-3 are shown in Figure 12. It can be seen that there is a high concentration of Cr element in the red-point region. The EDS result indirectly shows that the features observed on the fracture surface (Figure 11b-3) are sigma particles.

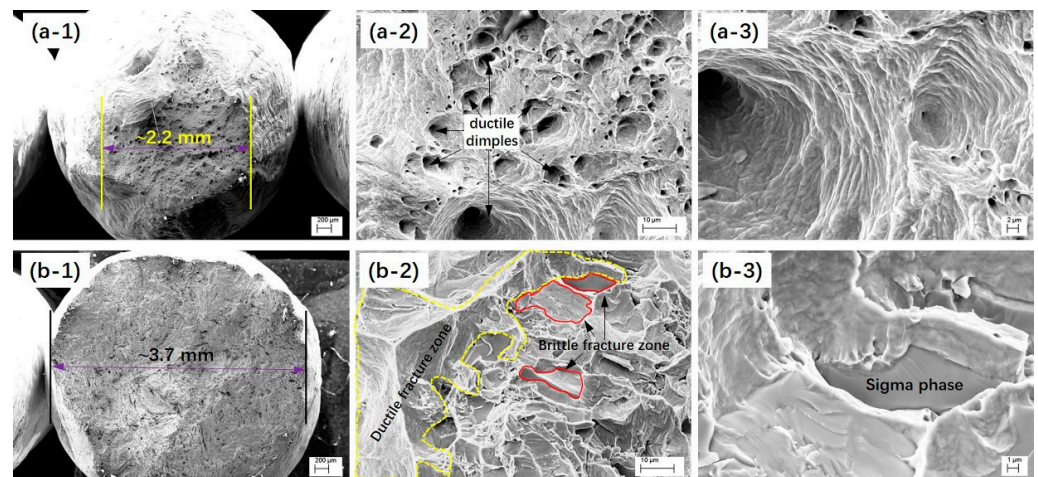


Figure 11. Tensile fracture surfaces of Z3CN20.09M specimens unaged (a) and aged at 750 °C for 200 h (b); 1—low magnification, 2—moderate magnification, and 3—high magnification.

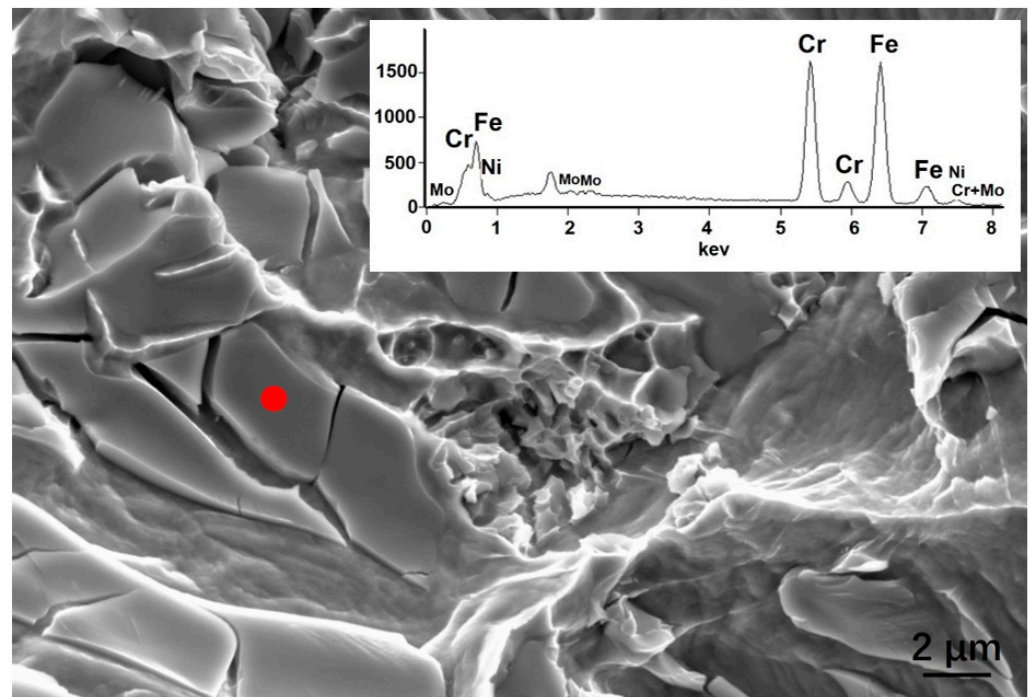


Figure 12. Fracture surface of aged Z3CN20.09M specimen and EDS results in the regions marked by red dot circle (insert).

4. Discussion

On the one hand, sigma is well known as one of the intermetallic compounds with a close-packed structure and is characterized by high hardness and brittleness. The hardness of the sigma is 17 GPa, examined through a nano indenter with a peak load of 500 μN [27]. Moreover, the elastic modulus of sigma is also very large [28] and up to 300 GPa in aged Z3CN20.09M tested with a nanoindentation instrument (see Figure 5). Therefore, the $(\sigma + \gamma_2)$ structures formed in Z3CN20.09M specimens by sigma precipitation due to the eutectoid decomposition of ferrite possess greater hardness than austenite and ferrite and can effectively inhibit the movement of dislocations and improve the strength of Z3CN20.09M steel due to their high thermodynamic stability at 350 °C. Therefore, the strength of aged Z3CN20.09M specimens containing $(\sigma + \gamma_2)$ structures is greater than that of unaged ones. According to the strength mixing law of steel [29], the more the

strengthening phases or structures are in steel, the higher the strength obtained. Thus, the strength of aged Z3CN20.09M specimens increased with increasing aging times due to the increase in sigma phases. However, the increase in strength of Z3CN20.09M specimens aged at 750 °C for longer than 50 h is slight. This is because the increase in sigma content of aged Z3CN20.09M specimens for 50 h to 200 h is not obvious (see Figure 8).

On the other hand, the precipitation of hard and brittle sigma phases brought more incoherent phase boundaries, including σ/γ_2 and $\alpha/\sigma/\gamma_2$. The more the sigma phases precipitated, the more σ/γ_2 and $\alpha/\sigma/\gamma_2$ phase boundaries formed. These boundaries are incoherent interfaces and are characterized by large mismatch, high interface energy, and low interface bonding strength [30–33]. Thus, these boundaries hindered the movement of dislocations and concentrated the stress during deformation, as shown in Figure 13, subsequently becoming potential crack sources that were prone to crack initiation. At the same time, the plastic deformation of the sigma phase is very difficult and releasing the stress concentration through plastic deformation is almost impossible. Therefore, cracks initiated easily at the σ/γ_2 or $\alpha/\sigma/\gamma_2$ boundaries and propagated rapidly when the aged specimen bore the ultimate load. Finally, the elongation at break of aged Z3CN20.09M specimens was lower than that of unaged ones and the fracture surface became brittle in aged specimens. Moreover, the longer the aging times, the less elongations at break.

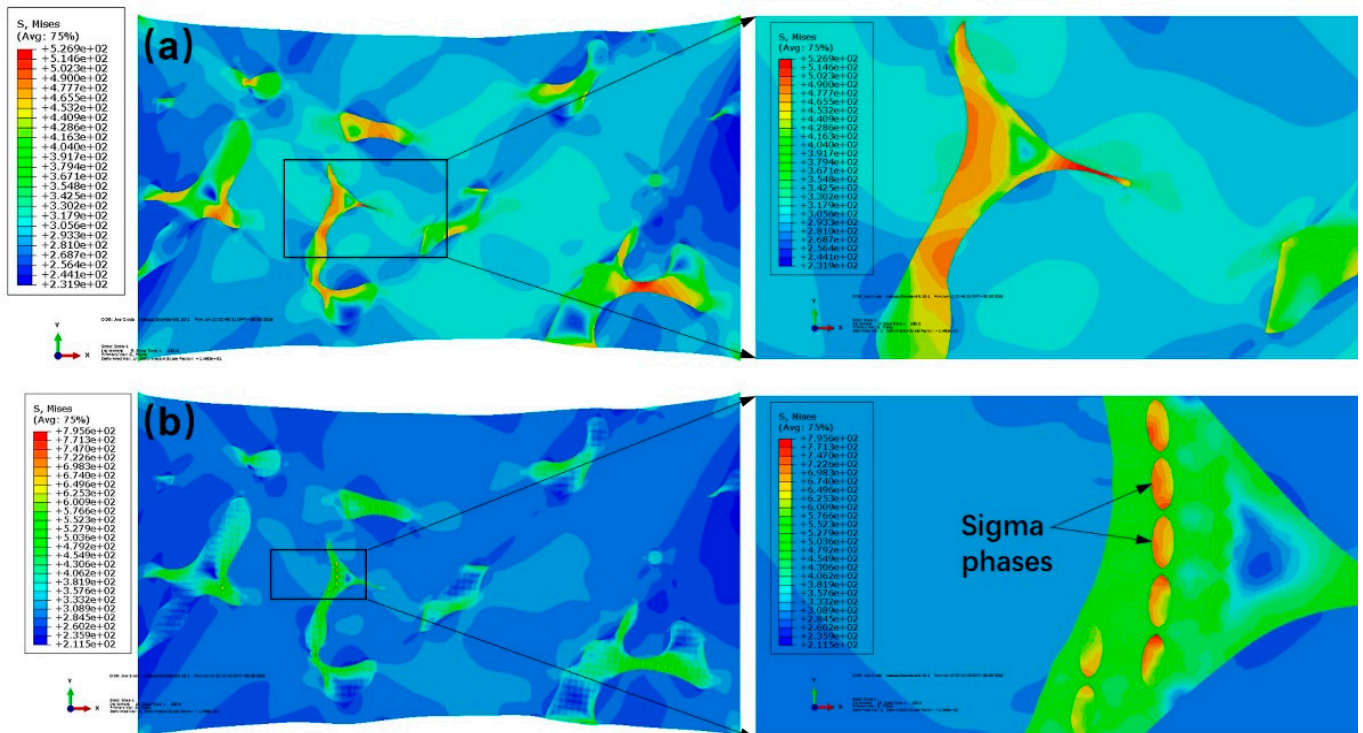


Figure 13. Calculated results of stress distribution in Z3CN20.09M specimens without (a) and with (b) sigma phases under tensile tests.

In addition, a significant effect of the sigma phase was seen on the strain hardening of Z3CN20.09M steel tensile tested at 350 °C. Dislocations were inhibited and accumulated at the interfaces of σ/γ_2 or $\alpha/\sigma/\gamma_2$ during plastic deformation due to the different crystal structures of the sigma, ferrite, and austenite phases. This resulted in an increase in the strain-hardening rate of aged Z3CN20.09M specimens. Therefore, at the stage of low strain during plastic deformation (true strain is below 0.117), the strain-hardening rate of aged Z3CN20.09M specimens was higher than that of unaged ones. The longer the aging times, the more coarse the sigma phases, so the higher the strain-hardening rate, as shown in stage I in Figure 14a. With increasing strain, however, the strain-hardening rate of aged Z3CN20.09M specimens was lower than that of unaged ones when the true strain exceeds

0.117. This is possible because the concentration of stress due to the accumulation of dislocations at the interfaces of σ/γ_2 or $\alpha/\sigma/\gamma_2$ with increasing strain becomes too large, to a certain extent, and subsequently initiates microcracks. At this stage, stress is released, the dislocation stacking degree decreased, and the strain-hardening rate also decreased. Notably, in the strain range of 0.117–0.176, the difference in the strain-hardening rate of aged Z3CN20.09M specimens for 50–200 h is very small, as shown in stage II in Figure 14a, although a difference in sigma content of aged specimens is still seen for different aging times. This may be due to the lower strain concentration, fewer microcracks, and less stress released. When the strain exceeds 0.176, the decrease in the strain-hardening rate of aged specimens is remarkable with the increase in strain at the high strain stage. The difference in the strain-hardening rate of aged specimens for different times is very significant. The longer the aging time, the lower the strain-hardening rate, as shown in stage III in Figure 14a. This is because the high strain causes the initiation and propagation of more microcracks and induces the release of more stress.

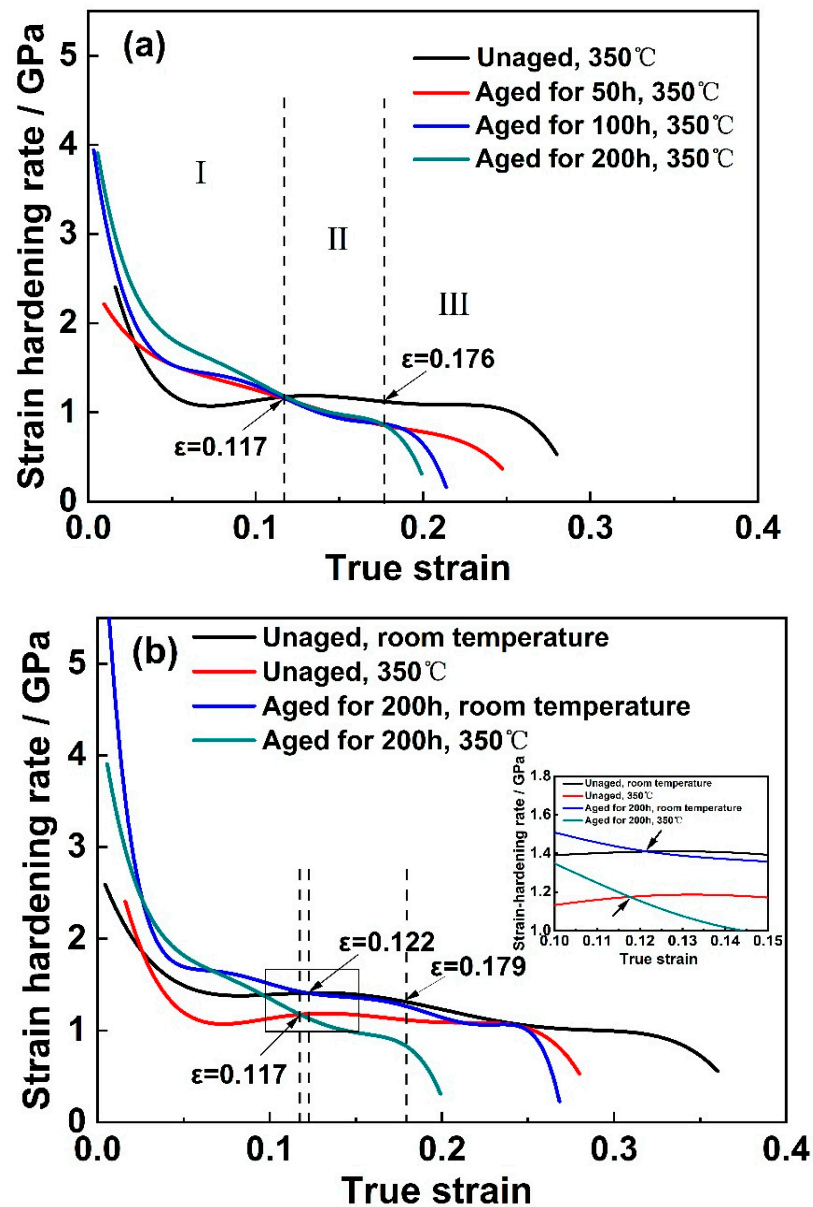


Figure 14. Strain-hardening rate of aged and unaged Z3CN20.09M specimens at different temperatures: (a) 350 °C, (b) 350 °C and room temperature.

Furthermore, the similar behaviors of the specimens, both aged and unaged, in stage II of room-temperature tests can be found, as shown in stage II in Figure 14b. In stage II of room-temperature tests, it is speculated that the boundaries of σ/γ_2 and $\alpha/\sigma/\gamma_2$, on the one hand, can hinder dislocation movement and bring the accumulation of dislocations and increase of stress; on the other hand, they can also provide the potential source of cracks initiation under a certain stress (or higher stress) and induce stress release. There is perhaps a balance of dislocation accumulation and stress release in stage II of aged material at room-temperature tests. Thus, the similar strain-hardening behaviors of aged and unaged specimens is displayed.

The effect of the sigma phase on the strain-hardening behavior of the Z3CN20.09M specimens tensile tested at moderate temperature is also different from that at room temperature. At a lower strain (below 0.117), the strain-hardening rate of aged specimens was higher than that of the unaged ones significantly tensile tested at 350 °C. This means that when the strain was below 0.117, the precipitation of the sigma phases improved the strain-hardening rate. However, when the strain exceeded 0.117, the strain-hardening rate of aged specimens with a sigma phase was less than that of unaged ones without sigma phases. Although a similar trend in the effect of sigma phases on the strain-hardening rate of Z3CN20.09M specimens tensile tested at room temperature was seen, the difference in the strain-hardening rate of aged and unaged specimens tensile tested at room temperature was smaller than that of those tensile tested at 350 °C. Notably, at a strain from 0.122 to 0.179, almost the same strain-hardening rate was found for aged and unaged specimens tensile tested at room temperature, while a distinct difference in the strain-hardening rate of aged and unaged specimens tensile tested at 350 °C was presented, as shown in Figure 14b. Obviously, the effect of the sigma phase on the hardening rate at moderate temperature was more significant, meaning that the strain-hardening rate at moderate temperature is more sensitive to the sigma phase. With rising temperature, the thermal activity of metallic atoms improved, the metallic bonds' strength became weaker, and the interfacial bonding strength boundaries of σ/γ_2 and $\alpha/\sigma/\gamma_2$ also became weaker. Under certain stresses, cracks initiate earlier and expand more easily at defects such as the σ/γ_2 and $\alpha/\sigma/\gamma_2$ phase interfaces, and the stress release is greater. Thus, the strain-hardening rate of aged specimens is much lower than that of unaged ones in stage II of 350 °C tests.

5. Conclusions

The precipitation of sigma phases in Z3CN20.09M CASS improved its strength and decreased plasticity after tensile testing at moderate temperature. A significant effect of the sigma phases was also seen on the strain-hardening rate. At a strain below 0.117, the strain-hardening rate of aged Z3CN20.09M specimens with sigma phases was higher than that of unaged ones without a sigma phase. With the increase in strain, however, the strain-hardening rate of aged Z3CN20.09M specimens was lower than that of unaged ones when the true strain exceeded 0.117.

No obvious necking after the rupture tensile tested at 350 °C was found in the macroscopic fracture surfaces of aged specimens containing sigma phases, which are characterized by typical brittle fracture. Microcosmically, many brittle rupture zones are found in the fractures. The brittle rupture zones occurred in the sigma phases, while remarkable necking appeared in the macroscopic fracture surfaces of unaged specimens without sigma phases, which are characterized by typical ductile fracture. Microcosmically, many ductile dimples with different sizes and depths were seen in the fracture of unaged specimens.

More significant effects are seen in the YS, UTS, and hardening rates in the sigma phase of Z3CN20.09M CASS that is tensile tested at moderate temperature than that at room temperature, meaning that the tensile mechanical properties of Z3CN20.09M CASS at moderate temperature are more sensitive to the sigma phase. This is due to the many high-energy phase boundaries of σ/γ_2 and $\alpha/\sigma/\gamma_2$ in aged Z3CN20.09M specimens after the precipitation of sigma phases, which are characterized by a high hardness, a high elastic modulus, and a significant difference in the crystal structure of the matrix.

Author Contributions: Conceptualization, Y.W.; software, S.L.; validation, C.H.; formal analysis, C.H.; investigation, S.L. and Z.G.; data curation, Z.G. and C.Z.; writing—original draft preparation, Y.W.; writing—review and editing, N.L.; supervision, N.L.; project administration, N.L. All authors have read and agreed to the published version of the manuscript.

Funding: This research was funded by the National Natural Science Foundation of China, grant numbers 51971003 and 52171059, and the Natural Science Foundation of Anhui Province, grant number 1508085QE102.

Institutional Review Board Statement: Not applicable.

Informed Consent Statement: Not applicable.

Data Availability Statement: The data presented in this study are available on request from the corresponding author. The data are not publicly available due to the data also forming part of an ongoing study.

Conflicts of Interest: The authors declare no conflict of interest.

References

1. Yamada, T.; Okano, S.; Kuwano, H. Mechanical property and microstructural change by thermal aging of SCS14A cast duplex stainless steel. *J. Nucl. Mater.* **2006**, *350*, 47–55. [[CrossRef](#)]
2. Cheng, H.T.; Guo, Y.R. Current situation and localization progress of pipes for nuclear power generation service. *Steel Pipe* **2008**, *37*, 1–5.
3. Zhao, Y.F.; Ti, W.X.; Wang, X.L.; Xue, F. Steel tubular materials for nuclear power plant service and production localization. *Steel Pipe* **2007**, *36*, 11–14.
4. Xue, F.; Wang, Z.X.; Shu, G.G.; Yu, W.W.; Shi, H.J.; Ti, W.X. Thermal aging effect on Z3CN20.09M cast duplex stainless steel. *Nucl. Eng. Des.* **2009**, *239*, 2217–2223. [[CrossRef](#)]
5. Kawaguchi, S.; Sakamoto, N.; Takano, G.; Matsuda, F.; Kikuchi, Y.; Mráz, L. Microstructural changes and fracture behavior of CF8M duplex stainless steels after long-term aging. *Nucl. Eng. Des.* **1997**, *174*, 273–285. [[CrossRef](#)]
6. Chopra, O.K.; Chung, H.M. Aging of cast duplex stainless steels in LWR systems. *Nucl. Eng. Des.* **1985**, *89*, 305–318. [[CrossRef](#)]
7. Mathew, M.D.; Lietzan, L.M.; Murty, K.L.; Shah, V.N. Low temperature aging embrittlement of CF-8 stainless steel. *Mater. Sci. Eng. A* **1999**, *269*, 186–196. [[CrossRef](#)]
8. Gunn, R.N. *Duplex Stainless Steels: Microstructure, Properties and Applications*; Abington Publishing: Cambridge, UK, 1997; p. 175.
9. Wang, Y.Q.; Han, J.; Wu, H.C.; Yang, B.; Wang, X.T. Effect of sigma phase precipitation on the mechanical and wear properties of Z3CN20.09M cast duplex stainless steel. *Nucl. Eng. Des.* **2013**, *259*, 1–7. [[CrossRef](#)]
10. Li, S.L.; Wang, Y.L.; Li, S.X.; Wang, X.T. Effect of long term aging on the microstructure and mechanical properties of cast austenitic stainless steels. *Acta. Metall. Sin.* **2010**, *46*, 1186–1191. [[CrossRef](#)]
11. Lo, K.H.; Shek, C.H.; Lai, J.K.L. Recent developments in stainless steels. *Mater. Sci. Eng. R* **2009**, *65*, 39–104. [[CrossRef](#)]
12. Sieurin, H.; Sandstrom, R. Sigma phase precipitation in duplex stainless steel 2205. *Mater. Sci. Eng. A* **2007**, *444*, 271–276. [[CrossRef](#)]
13. Magnabosco, R. Kinetics of sigma phase formation in a duplex stainless steel. *Mater. Res.* **2009**, *12*, 321–327. [[CrossRef](#)]
14. Chen, T.H.; Weng, K.L.; Yang, J.R. The effect of high-temperature exposure on the microstructural stability and toughness property in a 2205 duplex stainless steel. *Mater. Sci. Eng. A* **2002**, *338*, 259–270. [[CrossRef](#)]
15. Liu, F.X. σ Phase precipitation and its effect on mechanical properties of S32205 duplex stainless steel. *Iron Steel* **2010**, *45*, 62–65.
16. Pohl, M.; Storz, O.; Glogowski, T. Effect of intermetallic precipitations on the properties of duplex stainless steel. *Mater. Charact.* **2007**, *58*, 65–71. [[CrossRef](#)]
17. Shek, C.H.; Wong, K.W.; Lai, J.K.L.; Li, D.J. Hot tensile properties of 25Cr-8Ni duplex stainless steel containing cellular ($\sigma + \gamma_2$) structure after various thermal treatments. *Mater. Sci. Eng. A* **1997**, *231*, 42–47. [[CrossRef](#)]
18. Shek, C.H.; Li, D.J.; Wong, K.W.; Lai, J.K.L. Creep properties of aged duplex stainless steels containing σ phase. *Mater. Sci. Eng. A* **1999**, *266*, 30–36. [[CrossRef](#)]
19. Han, Y.S.; Hong, S.H. The effects of thermo-mechanical treatments on superplasticity of Fe-24Cr-7Ni-3Mo-0.14N duplex stainless steel. *Scripta. Mater.* **1997**, *36*, 557–563. [[CrossRef](#)]
20. Wang, Y.Q.; Han, J.; Yang, B.; Wang, X.T. Strengthening of σ phase in a Fe20Cr9Ni cast austenite stainless steel. *Mater. Charact.* **2013**, *84*, 120–125. [[CrossRef](#)]
21. Wang, Y.Q.; Yang, B.; Li, N.; Lin, S.H.; Sun, L. Embrittlement of σ phase in stainless steel for primary coolant pipes of nuclear power plant. *Acta. Metall. Sin.* **2016**, *52*, 17–24.
22. Zhao, Z.Y.; Xu, L.; Li, G.P.; Xue, R.D.; Zheng, J.H. Precipitation behavior of σ -phase and its effect on microstructure and properties of a super duplex stainless steel. *Trans. Mater. Heat. Treat.* **2010**, *31*, 75–79.
23. Wang, Y.Q.; Yang, B.; Han, J.; Wu, H.C.; Wang, X.T. Effect of precipitated phases on the pitting corrosion of Z3CN20.09M cast duplex stainless steel. *Mater. Trans.* **2013**, *54*, 839–843. [[CrossRef](#)]

24. Wang, Y.Q.; Li, D.D.; Sun, L.; Li, N.; Liu, M.K.; Shen, W.; Jing, H.M. Pitting corrosion of thermally aged cast duplex stainless steel for primary coolant pipes of nuclear power plants. *Corros. Eng. Sci. Techn.* **2017**, *52*, 447–452. [[CrossRef](#)]
25. Wu, H.C.; Yang, B.; Wang, Y.Q. Effect of sigma phase on the low cycle fatigue property of Z3CN20.09M cast duplex stainless steel in high temperature water. *Mater. Corros.* **2015**, *66*, 663–669. [[CrossRef](#)]
26. Wu, H.C.; Yang, B.; Chen, Y.F.; Chen, X.D. Effect of oxidation on the fatigue crack propagation behavior of Z3CN20.09M duplex stainless steel in high temperature water. *Nucl. Eng. Technol.* **2017**, *49*, 744–751. [[CrossRef](#)]
27. Wang, Y.Q.; Han, J.; Yang, B.; Wu, H.C.; Wang, X.T. Precipitation behavior of the intermetallic phases in Z3CN20.09M stainless steel for primary coolant pipes of nuclear power plant. *Acta Metall. Sin.* **2013**, *49*, 415–420. [[CrossRef](#)]
28. Ohmura, T.; Tsuzaki, K.; Sawada, K.; Kimura, K. Inhomogeneous nano-mechanical properties in the multi-phase microstructure of long-term aged type 316 stainless steel. *J. Mater. Res.* **2006**, *21*, 1229–1236. [[CrossRef](#)]
29. Yao, Y.; Zhou, C.D.; Shi, B.; Yang, X.P.; Shan, A.D.; Song, H.W. Nanoindentation characterization of mechanical properties of σ phase in super duplex stainless steel. *Mater. Mech. Eng.* **2011**, *35*, 1–7.
30. Kumar, A.; Singh, S.B.; Ray, K.K. Influence of bainite/martensite-content on the tensile properties of low carbon dual-phase steels. *Mater. Sci. Eng. A* **2008**, *474*, 270–282. [[CrossRef](#)]
31. Ashby, M.F. Work hardening of dispersion-hardened crystals. *Philos. Mag.* **1966**, *14*, 1157–1178. [[CrossRef](#)]
32. Ooi, S.W.; Hill, P.; Rawson, M.; Bhadeshia, H.K.D.H. Effect of retained austenite and high temperature Laves phase on the work hardening of an experimental maraging steel. *Mater. Sci. Eng. A* **2013**, *564*, 485. [[CrossRef](#)]
33. Viswanathan, U.K.; Dey, G.K.; Asundi, M.K. Precipitation hardening in 350 grade maraging steel. *Metall. Trans. A* **1993**, *24*, 2429–2442. [[CrossRef](#)]

Disclaimer/Publisher’s Note: The statements, opinions and data contained in all publications are solely those of the individual author(s) and contributor(s) and not of MDPI and/or the editor(s). MDPI and/or the editor(s) disclaim responsibility for any injury to people or property resulting from any ideas, methods, instructions or products referred to in the content.